

# Nanoscale

Accepted Manuscript



This is an *Accepted Manuscript*, which has been through the Royal Society of Chemistry peer review process and has been accepted for publication.

*Accepted Manuscripts* are published online shortly after acceptance, before technical editing, formatting and proof reading. Using this free service, authors can make their results available to the community, in citable form, before we publish the edited article. We will replace this *Accepted Manuscript* with the edited and formatted *Advance Article* as soon as it is available.

You can find more information about *Accepted Manuscripts* in the [Information for Authors](#).

Please note that technical editing may introduce minor changes to the text and/or graphics, which may alter content. The journal's standard [Terms & Conditions](#) and the [Ethical guidelines](#) still apply. In no event shall the Royal Society of Chemistry be held responsible for any errors or omissions in this *Accepted Manuscript* or any consequences arising from the use of any information it contains.

Cite this: DOI: 10.1039/c0xx00000x

www.rsc.org/xxxxxx

ARTICLE TYPE

## Ultra-bright Alkylated Graphene Quantum Dots

Lan Feng, Xing-Yan Tang, Yun-Xin Zhong, Yue-Wen Liu, Xue-Huan Song, Shun-Liu Deng,\* Su-Yuan Xie, Jia-Wei Yan, and Lan-Sun Zheng

Received (in XXX, XXX) Xth XXXXXXXXX 20XX, Accepted Xth XXXXXXXXX 20XX

DOI: 10.1039/b000000x

Highly efficient and stable photoluminescence (PL) are urgently desired for graphene quantum dots (GQDs) to facilitate their prospective applications as optical materials. Here, we report the facile and straightforward synthesis of alkylated graphene quantum dots (AGQDs) via the solvothermal reaction of propagatively alkylated graphene sheets (PAGenes). In contrast to most GQDs reported so far, the synthesized AGQDs process pH-independent and ultra-bright PL with a relative quantum yield up to 65%. Structural and chemical composition characterization demonstrated that the synthesized AGQDs are nearly oxygen-defect-free with alkyl groups decorated on edges and basal plane, which may contribute to their greatly improved pH tolerance and high quantum efficiency. The photocatalytic performance of AGQDs-P25 nanocomposites was evaluated by the degradation of Rhodamine B under visible light. The photocatalytic rate is *ca.* 5.9 times higher than that of pure P25, indicating that the AGQDs could harness the visible spectrum of sunlight for energy conversion or environmental therapy.

### Introduction

In the past decade, there has been an explosion of graphene research in the field of nanoscience and nanotechnology for its unique structure and excellent properties.<sup>1</sup> However, graphene is not photoluminescent for the lack of electronic bandgap, which limits its application in optoelectronics. Through surface modification methods, the electronic structure of graphene could be tuned giving rise to fluorescent materials,<sup>2-4</sup> whereas the large size of graphene sheets and the low quantum efficiency impede their direct application in nanodevices. In addition to their intrinsic properties of graphene, graphene quantum dots (GQDs), which are disc-like graphene pieces with lateral sizes less than 100 nm, exhibit new optical properties due to quantum confinement and edge effects.<sup>5-7</sup> In comparison with organic dyes and semiconductive quantum dots, GQDs are superior in terms of large optical absorptivity, high chemical stability, fine biocompatibility, and low toxicity,<sup>8-10</sup> showing promising applications in photovoltaic devices,<sup>11-13</sup> bioimaging,<sup>14-16</sup> photoluminescent sensors,<sup>17, 18</sup> and photocatalysis.<sup>19, 20</sup>

So far methods such as organic synthesis starting from special organic precursors<sup>12, 21-23</sup> or physical producing including high-resolution electron-beam nanolithography and cage-opening of fullerene are successful in producing GQDs for fundamental research.<sup>5, 24</sup> However, complicated synthetic route, expensive equipments, poor solubility, and low throughput remain limiting

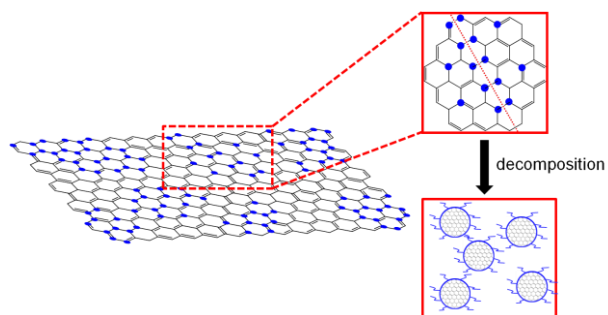
factors for these methods in producing large quantities of GQDs needed for many prospective applications. Alternatively, GQDs can be synthesized from various carbon-based materials including graphite or graphene oxides (GOs),<sup>11, 15, 19, 25-32</sup> carbon nanotubes,<sup>33, 34</sup> carbon fibers,<sup>16</sup> carbon black,<sup>35</sup> and coal<sup>36</sup> by chemical cutting routes. Although much progress has been made, including abundant raw materials, simple operation, and improved solubility of GQDs, these methods have limitations to overcome: Firstly, GQDs fabricated by these methods usually suffered from low synthetic yield and heterogeneity in size and shape. Time consuming dialysis or chromatography separation was usually required to obtain desired products. Secondly, before chemical cutting, the carbon-based materials required harsh oxidation for a long time, resulting in a large content of oxygen defects on their structures. GQDs fabricated from these oxidized precursors are known to remain abundant oxygen-containing functional groups such as epoxides, hydroxyl, carbonyl, and carboxyl groups. Strictly speaking, they are graphene oxide quantum dots rather than graphene quantum dots.<sup>37</sup> Although GQDs could readily disperse in water or polar solvents such as N,N-dimethylformamide (DMF), the hydrophilic surface property limited their dispersibility in nonpolar solvents. Last but not least, highly efficient and stable photoluminescence (PL) is crucial for GQDs to facilitate their prospective applications as optical materials. However, the fluorescent quantum yield of GQDs is quite low (less than 10%) if no further chemical doping, passivation and/or reduction is made. Moreover, the PL behaviors of GQDs exhibit low pH tolerance, limiting their practical application in the solution of high or low pH value.

Hence, in addition to a more facile and reliable synthetic method, a much more stable PL with higher quantum yield is highly desired for GQDs to facilitate their prospective application

Department of Chemistry, State Key Laboratory of Physical Chemistry of Solid Surface, College of Chemistry and Chemical Engineering, Xiamen University, Xiamen, 361005, China. E-mail: sldeng@xmu.edu.cn

† Electronic Supplementary Information (ESI) available: additional figures (Fig. S1-S12). See DOI: 10.1039/b000000x/

as optical materials. Based on a fundamental understanding of graphene chemistry and functionalization patterns on  $sp^2$  carbon lattice, we recently reported the large-scale exfoliation and controlled functionalization of graphene sheets.<sup>38, 39</sup> The propagatively alkylated graphene sheets (PAGenes) exhibit an interesting “islanded” structure containing intact and functionalized regions, with smaller  $sp^2$  domains interlaced with  $sp^3$  regions. Here we show that the one-pot solvothermal treatment of PAGenes in organic solvents such as DMF resulted in the decomposition of microsized graphene sheets, giving rise to ultrafine alkylated graphene quantum dots (AGQDs) (Scheme 1). In comparison with the previously reported GQDs, the synthetic yield and the homogeneity in size and shape of AGQDs were considerably improved. The synthesized AGQDs show excellent dispersibility in water and common organic solvents without further surface modification, including polar and nonpolar solvents. Significantly, the AGQDs exhibit pH-independent and ultra-bright PL with quantum yield up to 65%, which places them among the brightest-reported ensembles of GQDs. Structural and composition characterizations suggest that the synthesized AGQDs are nearly oxygen-defect-free with alkyl groups decorated on edges and basal plane, which may contribute to their ultra-bright and pH-independent PL. The degradation experiments of Rhodamine B show that the photocatalytic rate of AGQDs-P25 nanocomposites is *ca.* 5.9 times higher than that of pure P25 under visible light ( $\lambda > 420$  nm) irradiation.



**Scheme 1** Schematic illustration of the solvothermal decomposition of PAGenes. The blue spots in graphene sheets are alkylated ( $sp^3$ ) carbon atoms (For clarity, the attached alkyl functional groups are omitted).

## Experimental

### Materials

Graphite powder ( $< 5 \mu\text{m}$ ) was purchased from Nanjing XFNANO Materials Tech Co., Ltd. (Nanjing, China). 1-bromododecane (98%) was purchased from Sinopharm Chemical Reagent Co., Ltd. (Shanghai, China). Methyl 6-bromohexanoate (98%) were purchased from Accela ChemBio Co., Ltd. (Shanghai, China).  $\text{TiO}_2$  (P25), which contained 20% rutile and 80% anatase, was purchased from Degussa. Other chemicals and solvents were commercially available and used as received.

### Preparation of propagatively alkylated graphene sheets (PAGenes)

PAGenes were prepared by recycling reductive alkylation as reported in our previous works.<sup>38-40</sup> When 1-bromododecane and methyl 6-bromohexanoate were used as alkyl halide agents, the

products were named PAGenes and PAGenes-COOR, respectively.

### Preparation of alkylated graphene quantum dots (AGQDs)

AGQDs were prepared from PAGenes by solvothermal route. Specifically, 3 mg of PAGenes were dispersed in 40~50 mL of DMF by mild sonication for 3 h, after which the dispersion was transferred to a Teflon-lined autoclave. The autoclave was sealed and maintained at 200 °C for 20 h. After reaction, the products were cooled down to room temperature. The resultant brown-yellow transparent supernatant and black precipitates were collected respectively for characterization. In this work, AGQDs were also fabricated from PAGenes-COOR in identical solvothermal conditions.

### Preparation of oxidized alkylated graphene quantum dots (OAGQDs)

In order to investigate the effect of oxygen-containing functional groups on the optical properties of AGQDs, the synthesized AGQDs were performed oxidization using modified Hummers method.<sup>41</sup> Specifically, concentrated  $\text{H}_2\text{SO}_4$  (10 mL 98%) was slowly added to a mixture of AGQDs (10 mg) and  $\text{NaNO}_3$  (145.0 mg) in a round-bottom flask within an ice bath. After that,  $\text{KMnO}_4$  (35.2 mg) was gradually added and the mixture was continuously stirred for 30 min. After the addition of 25 mL deionized water, the solution was stirred for further 30 min. Subsequently, 5 mL  $\text{H}_2\text{O}_2$  (30%) was added to reduce the residual  $\text{KMnO}_4$ . The reaction was allowed to react for 30 min, followed by the addition of 50 mL deionized water. The final solution was dialyzed in a dialysis bag (retained molecular weight: 1000 Da) to obtain OAGQDs.

### Preparation of AGQDs-P25 nanocomposites and photocatalytic activity studies

P25  $\text{TiO}_2$  (50 mg) was dispersed in 30 mL of AGQDs aqueous solution with a concentration of 0.2 mg/mL by stirring for 30 min, after which the mixture was transferred to a Teflon-lined autoclave and heated at 150 °C for 6 h. The yellow-brown products were collected by centrifugation at 6000 rpm for 5 min and washed with copious water. The final solid was then dried in a vacuum oven at 70 °C for 10 h to yield AGQDs-P25 nanocomposites.

The photocatalytic activity of the as-prepared AGQDs-P25 nanocomposites was evaluated by the photocatalytic degradation of Rhodamine B under 300 W Xe lamp irradiation (PLS-SXE300, Beijing Trustech Co., Ltd) with a 420 nm cutoff filter at room temperature. Specifically, 50 mg AGQDs-P25 composites were added into 50 mL of Rhodamine B aqueous solution (10 ppm). Before illumination, the suspension was stirred for 2 h in dark to ensure the adsorption-desorption equilibrium between the photocatalysts and Rhodamine B. Then, the solution was stirred for 90 min under visible light irradiation. At designated intervals, 2 mL of the solution was extracted and centrifuged to separate the photocatalyst particles (14000 rpm, 10 min). The concentration of Rhodamine B was measured by UV-Visible absorption spectroscopy with the characteristic absorption at  $\lambda_{\text{max}} = 553$  nm.

The photocatalytic activity of pure P25 and AGQDs was evaluated in a similar way as a control.

### Characterization

5 Scanning Electron Microscopy (SEM) images and energy-dispersive X-ray (EDS) element mapping were obtained on a Hitachi S-4800 scanning electron microscope. Transmission Electron Microscopy (TEM) images were obtained on a TECNAI F-30 transmission electron microscope. Atomic Force  
10 Microscope (AFM) images were taken on an Agilent 5500 AFM instrument (Agilent Technologies) in tapping mode. X-ray diffraction (XRD) patterns were recorded on a Rigaku Ultima IV diffractionmeter with Cu-K $\alpha$  radiation ( $\lambda = 1.5418 \text{ \AA}$ ) and a  
15 10 %/min. Raman spectra were obtained on a Renishaw Invia Raman microscope using a 532 nm excitation line. Fourier transform infrared (FT-IR) spectra were recorded on a Nicolet 380 FT-IR spectrometer. Thermogravimetric analysis (TGA) was performed on a SDT Q600 thermogravimetric analysis (TGA)  
20 instrument in the temperature ranging from 30 to 600 °C at a heating rate of 10 °C/min in N<sub>2</sub> atmosphere. X-ray photoelectron spectroscopy (XPS) was performed on a Quantum 2000 spectrometer, and the Al-K $\alpha$  line was used as the excitation source. Absorption spectra were recorded on a Shimadzu UV-  
25 2550 absorption spectrometer using 1 cm quartz cuvettes. Emission spectroscopy was performed on an F-7000 fluorescence spectrophotometer.

### Results and discussion

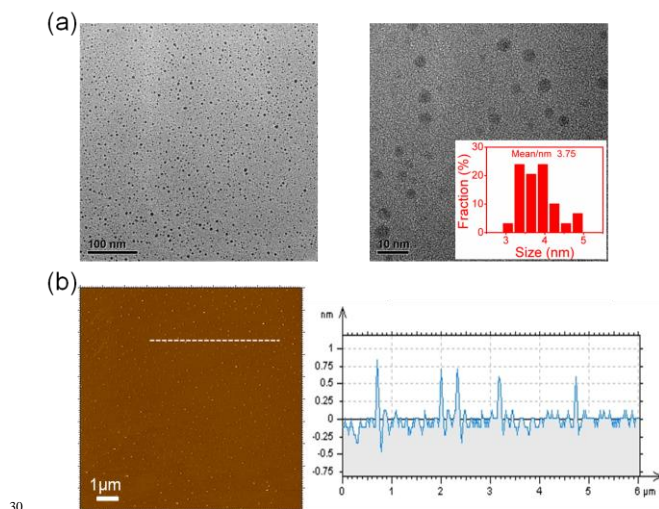


**Fig. 1** AGQDs formed in transparent supernatant after solvothermal reaction of PAGenes. (a) TEM images and size distribution of AGQDs. (b) AFM image and the corresponding height profile of a line scan.

Fig. 1a shows the typical TEM images and size distribution of  
35 AGQDs obtained in the transparent supernatant after solvothermal reaction of PAGenes. Their diameters are mainly distributed in the range of 3-5 nm with an average size of 3.75 nm. This result indicates that the monodisperse AGQDs are much smaller than GQDs synthesized from GOs by hydrothermal  
40 (around 9.6 nm) and solvothermal (around 5.3 nm) routes.<sup>15, 25</sup>

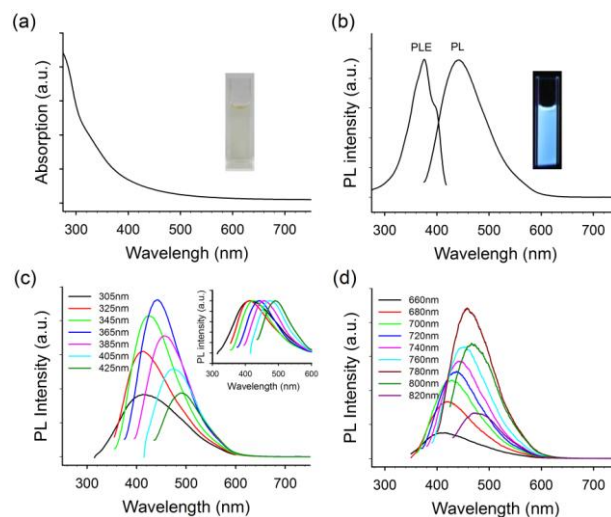


**Fig. 2** Optical properties of AGQDs. (a) UV-Vis absorption spectrum of AGQDs in DMF (inset: photograph taken under visible light), (b) PL at 365 nm excitation and PLE with the detection wavelength of 440 nm of AGQDs (inset: photograph taken under 365 nm UV light irradiation), (c) the excitation-dependent PL behavior of AGQDs (inset: normalized to the spectral peaks), and (d) the upconversion PL properties of AGQDs.

AFM image (Fig. 1b) shows that their average height is  $\sim 0.5$ -1.0 nm, indicating that the synthesized AGQDs consist of 1-2  
50 graphene layers.

The optical properties of the synthesized AGQDs were explored by ultraviolet-visible (UV-Vis) absorption spectroscopy and PL spectroscopy. As shown in Fig. 2a, the featureless absorption spectrum of AGQDs dispersed in DMF expands along the whole  
55 visible region with a shoulder feature at *ca.* 340 nm. Inset in Fig. 2b is a photograph of the dispersed AGQDs illuminated under 365 nm UV lights. The bright blue PL is strong enough to be seen by the naked eye. To further explore the optical properties of AGQDs, a detailed PL study was performed under different  
60 excitation wavelengths. Fig. 2c shows normal and normalized PL spectra of AGQDs. The AGQDs show an excitation-dependent PL behavior, in which the PL peak shifts to longer wavelength when the excitation wavelength is changed from 305 to 425 nm. The strongest PL appears at 440 nm upon 365 nm excitation,  
65 which is consistent with their PL excitation (PLE) spectrum (Fig. 2b). This phenomena is consistent with previous fluorescence analysis of GQDs.<sup>11, 15, 25, 27, 28</sup> In addition to the strong downconversion PL, the synthesized AGQDs also possess upconversion PL property. As shown in Fig. 2d, when excited from 660 nm to 820 nm, the upconversion PL exhibits similar excitation-dependence compared to that shown for short wavelength excitation (downconversion). The clear upconversion PL behavior makes AGQDs promising candidates for the design  
70 of photocatalysts to harness the visible spectrum of sunlight for energy conversion and environmental therapy (*vide infra*).<sup>19</sup>

The black precipitates formed in the solvothermal reaction of PAGenes were also performed detailed characterization without further separation. It is interesting to find that the precipitates can readily disperse in pure DMF by hand-shaking, yielding a  
80 transparent brown-yellow dispersion (inset in Fig. S2a). The representative TEM images show that most of the products are ultrafine well-dispersed particles (Fig. S1a) with diameter distributing in the range of 2-6 nm (the average diameter is 4.02

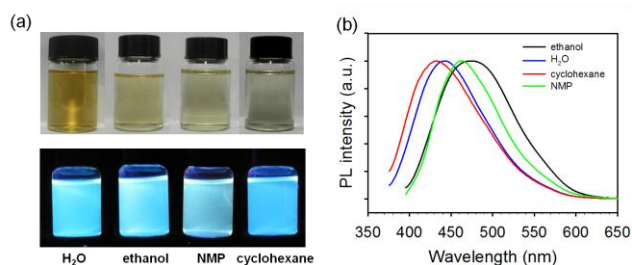


**Fig. 3** AGQDs dispersion in water, ethanol, NMP, and cyclohexane. (a) Photos taken under visible light (upper) and 365 nm UV light irradiation (lower), (b) PL of AGQDs dispersed in different solvents under optimal excitation.

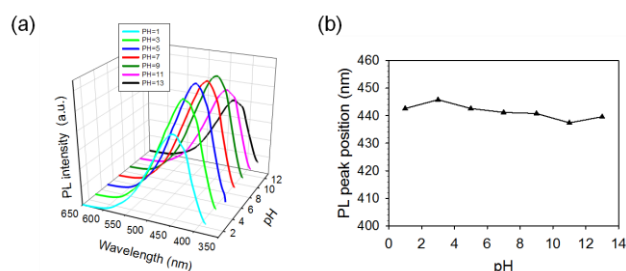


**Fig. 4** (a) PL of AGQDs in diverse pH solutions, (b) PL peaks wavelength of AGQDs at different pH conditions. PL spectra are collected at optimal 360 nm excitation.

nm). Their height is about 0.5~1.25 nm. Consequently, it is concluded that most of products in precipitates are single layered or few-layered (2-3 layers) GQDs. In addition to the similarity in morphology, the optical properties of the GQDs are spectrally identical with those of AGQDs formed in supernatant (Fig. S2). Accordingly, we expect that the products formed in supernatant and precipitates share similar size and chemical composition.

Apart from DMF, it is worth noting that the synthesized AGQDs can also dissolve in water and other organic solvents without further modification, including polar and nonpolar solvents. Shown in Fig. 3 are AGQDs dispersions in water, ethanol, N-methylpyrrolidone (NMP), and cyclohexane, respectively. Under 365 nm UV light irradiation, all without exception emit bright blue PL. TEM (Fig. S3) and optical properties characterization (Fig. S4) indicate their monodisperse morphology and excitation-dependent PL behavior. Under optimal excitation, the AGQDs dispersed in water, ethanol, NMP, and cyclohexane show PL peak at 440, 474, 462, and 431 nm, respectively (Fig. 3b). The observed solvent-dependent fluorescence property of AGQDs is consistent with that of GQDs, which could be explained by the adsorption of solvent on their surface.<sup>15</sup> The excellent dispersibility in both polar and nonpolar solvents makes AGQDs superior to GQDs in practical applications.

The synthesized AGQDs display some important properties existing in GQDs, such as excellent solubility, solvent- and excitation-dependent emission, and up-conversion PL behavior. However, some unexpected properties were also observed in AGQDs. For example, unlike GQDs, which process mutable emission color from blue to green depending on the degree of surface oxidization, the synthesized AGQDs process single emission color (blue) independent on their functional groups (Fig. S5). Using Rhodamine B as a reference, the PL quantum yield of AGQDs was measured to be ~ 65% (Table S1), which is considerably higher than that of luminescent GQDs (less than 10%). Moreover, the AGQDs exhibit interesting pH-independent PL behaviors. Fig. 4 shows the fluorescence of AGQDs in diverse pH solutions. Despite a minor decrease at high (pH = 11 and 13) and low pH (pH = 1), the PL of AGQDs was found stable and the wavelength kept around 440 nm. In contrast, the PL behaviors of GQDs are heavily dependent on the pH condition.<sup>16, 25</sup> For example, under alkaline conditions, GQDs emit strong PL, whereas under acidic conditions, the PL is completely quenched. The different PL behaviors between AGQDs and GQDs reflect different origins of luminescence, which is closely related to their structural characteristics.

Several characterization techniques were adopted to reveal the structure and chemical composition of the synthesized AGQDs. The solution <sup>1</sup>H NMR spectrum of AGQDs dispersed in CDCl<sub>3</sub> is shown in Fig. S6, in which the signals for aliphatic -CH<sub>2</sub>- at 1.26 and -CH<sub>3</sub> at 0.89 ppm clearly prove the presence of alkyl chains in AGQDs. The chemisorbed alkyl groups was further confirmed by thermogravimetric analysis (TGA). As shown in Fig. S7, AGQDs exhibit two weight loss peaks at ~290 °C and ~500 °C, which can be attributed to the desorption of solvents and decomposition of alkyl groups in AGQDs at elevated temperature, respectively. XPS measurements were also performed to determine the chemical composition of AGQDs. As shown in Fig. 5a, the XPS survey scan spectrum shows a dominating graphitic C1s peak at ca. 284.5 eV with a weak oxygenous peak at ca. 532 eV. The C1s high resolution XPS spectrum reveals that the peak consists of two major components at 284.5 and 285.1 eV, which can be identified with the sp<sup>2</sup> (C=C) and sp<sup>3</sup> (C-C) hybrid forms of carbon, respectively (Fig. 5b). The content of C-O is almost negligible. This result indicates that the sample contains negligible oxygen-containing groups. The FTIR spectrum is shown in Fig. 5c. The alkyl C-H stretching (~2800-3000 cm<sup>-1</sup>) and deformation (~1380-1470 cm<sup>-1</sup>) modes unambiguously confirm the presence of alkyl chains in AGQDs. The peak at ~1576 cm<sup>-1</sup> is assigned to the stretching vibration of C=C in the basal plane of AGQDs. It worth noting that no distinct peaks associated with oxygen-containing functional groups such as epoxides, hydroxyl, and carboxyl groups were observed, which is consistent with the XPS analysis. Raman spectrum of AGQDs is shown in Fig. 5d. The peak at ~1355 cm<sup>-1</sup> is D-band, related to the presence of sp<sup>3</sup>-type defects and edge defects. The peak at ~1590 cm<sup>-1</sup> is G peak, related to the in-plane vibration of sp<sup>2</sup> hybridized carbons. The relative intensity ratio of the D-band to G peak ( $I_D/I_G$ ) was 1.1. The Raman spectrum of AGQDs also shows a strong and symmetric 2D peak at ~2700 cm<sup>-1</sup>, indicating that the synthesized AGQDs are single or few-layer (< 3 layers),<sup>42</sup> which is consistent with the AFM measurement.

Although GQDs could be fabricated from GOs via hydrothermal and solvothermal routes, the synthetic yield of GQDs was very limited.<sup>15, 25-27</sup> Tedious separation process was usually required to obtain desired products from suspension, whereas the precipitates primarily containing not fully cut graphene flakes were wasted. In contrast, using PAGenes as starting materials, ultrafine AGQDs were directly obtained in both supernatant and precipitates without further separation. When PAGenes was replaced by PAGenes-COOR, we found similar trends of decomposition and fluorescent AGQDs (Fig. S5).

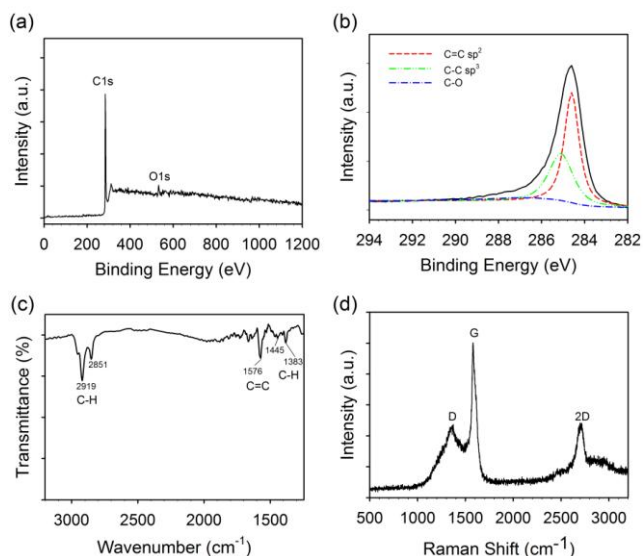


**Fig. 5** Structural and chemical composition characterization of AGQDs. (a) XPS survey scan spectrum, (b) C 1s high resolution XPS spectrum, (c) FTIR spectrum, and (d) Raman spectrum.

5 These results indicate that the framework of PAGene is more fragile than that of GO, tending to break up into small pieces in solvothermal conditions. To show the advantage of PAGenes over GOs for synthesizing GQDs, we treated GOs obtained by a modified Hummers method<sup>43</sup> under the same solvothermal  
10 conditions as that we used for PAGenes. As shown in Fig. S8, although the dosage of GOs is ten times the weight of PAGenes, the color of dispersion is much lighter than that of PAGenes, indicating the low cutting efficiency and low concentration of GQDs.

15 In GOs, the cooperative alignment of epoxy chains already formed during acid oxidization made graphene sheets fragile to rupture into smaller pieces in hydrothermal and solvothermal deoxidization process.<sup>25,44</sup> However, in stark contrast to the harsh oxidization chemistry of GOs, PAGenes were fabricated by  
20 reductive alkylation,<sup>45,46</sup> during which alkyl functional groups were propagatively attached on graphene layer. Structural and chemical composition characterization such as XPS, FTIR, and Raman proved that the graphene sheets were heavily functionalized by alkyl chains with negligible oxygen defects  
25 (Fig. S9). Therefore, it is undoubtedly concluded that the rupture of PAGenes is not induced by epoxy chains as that of GOs.

Theoretical studies has shown that the final shape of nanoscale carbon structures can be manipulated by their surface modification.<sup>47</sup> For example, the linear and hydrogenated  $sp^3$   
30 carbon-carbon single bonds converted by hydrogenation on graphene layer show an ability to disassemble the original structure by cutting it along the line of the modified bonds. Although the detailed cutting mechanism of PAGenes is not clear, this unzipping mechanism for carbon nanostructures may provide  
35 us an understanding of the structural transformation of PAGenes in solvothermal conditions.

We have recently reported that reductive alkylation occurs on graphene structure by defect activation, converting the modified carbon atoms from  $sp^2$  hybridization to  $sp^3$ .<sup>38</sup> The introduced  $sp^3$   
40 defects can act as new defect centers for continued propagation of the reaction fronts, resulting in the propagative alkylation of

graphene sheets. Through reaction propagation that starts at edge defects or defects initially present in graphene layer, the large  $sp^2$  domain in graphene is gradually broken into small conjugated  
45 systems separated by  $sp^3$  hybridized carbons.<sup>39</sup> As reaction propagating, the fraction of  $sp^3$  carbons is expected to increase. If three or more pairs of alkylated C-C single bonds form a line as presented in Scheme 1, the middle C-C bond from the line of alkylated atoms shows high propensity to break due to the  
50 distortion of graphene lattice. On one hand, alkylation changed the hybridization of carbon atoms connected by the C-C bond from  $sp^2$  hybridization to  $sp^3$ , enlarging the bond length from 1.42 to 1.52 Å. Therefore, the strength of such a C-C bond is significantly weakened. On the other hand, alkylation caused  
55 graphene lattice distortion such that the carbon atoms alkylated from different sides of graphene are shifted out of graphene plane in opposite directions. The tensile stress arising at the modified C-C bond induced by lattice distortion further reduced its strength. For the first and last pairs, the tensile stress could be compensated  
60 by neighbor unmodified graphene lattice, whereas the tensile stress arising at the middle pair has the ability to break the C-C bond. Some ultrafine pieces surrounded by the alkylated C-C bond lines may further break up in the solvothermal conditions. Thus the micrometer-sized graphene sheets ruptured to give  
65 nanometer-sized AGQDs with edge-terminated by alkyl groups, although the decoration of alkyl groups on basal plane is also possible. The attachment of alkyl groups renders the formed ultrafine AGQDs excellent solubility in DMF to give transparent supernatant, while the formation of precipitates can be explained  
70 by the concentration limit of AGQDs in DMF. As a proof, a transparent dispersion was readily obtained by hand-shaking them in pure DMF (inset in Fig. S2a), with very little sediment even after four months.

GQDs fabricated from GOs by chemical cutting routes process  
75 a high degree of oxidation with hydroxyl, epoxy, carbonyl, and carboxylic groups decorated on surface. Although the fluorescence mechanism is not fully understood, it is generally considered that the PL of GQDs is derived from the combination effect of intrinsic state emission and surface defect state  
80 emission, in which the former is related to quantum size effect, zigzag sites, and the radiative recombination of localized electron-hole pairs, while the later is attributed to oxygen-containing functional groups and any sites other than perfect  $sp^2$  domains.<sup>48,49</sup> In general, intrinsic state contributes to blue color  
85 emission and surface defect state is the common origin of green luminescence of GQDs.<sup>37,50</sup> Since the surface defects of GQDs intensely varied with their synthesis and post-treatment process, the contribution of each state emission on the PL of GQDs is hard to control, which may result in the mutable emission color of  
90 GQDs from blue to green. Moreover, the surface oxygen-containing functional groups such as  $-COOH$  and epoxy can always induce non-radiative recombination of localized electron-hole pairs, holding back the intrinsic state emission.<sup>49</sup> This can partially explain the low quantum yield of GQDs. Chemical  
95 doping is an effective way to increase their quantum yields,<sup>51-53</sup> whereas the incorporation of heteroatoms would disrupt the intrinsic structure of graphene lattice. Surface passivation and/or reduction were also applied to modulate the surface states of GQDs,<sup>28-30,49,54-58</sup> by which the intrinsic state emission was

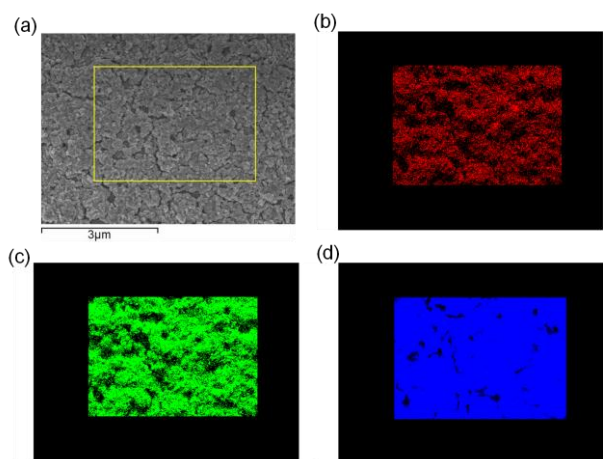


**Fig. 6** (a) SEM image of AGQDs-P25 nanocomposites, and EDS element mapping data of (b) C, (c) O, and (d) Ti elements of the region indicated by the yellow box in part (a).

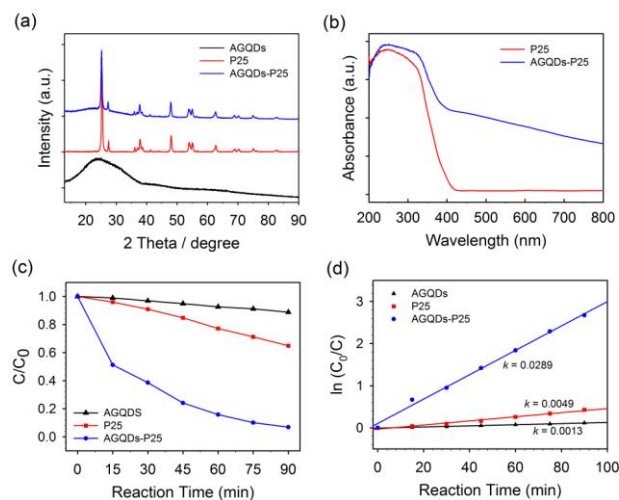


**Fig. 7** (a) XRD patterns of P25, AGQDs, and AGQDs-P25, (b) UV-Visible diffuse reflectance spectra of P25 and AGQDs-P25 nanocomposites films, and (c, d) photocatalytic performance of different catalysts.

enhanced changing the emission light color from green to blue, and their fluorescent quantum yields could be subsequently increased over 40%. For example, upon surface aryl-modification, the quantum yield of GQDs was increased from 1.0% to 7.0%,<sup>55</sup> while the quantum yield of amino-functionalized GQDs was ~46%.<sup>30</sup> However, despite the surface passivation or reduction process, there was a certain level of oxygenous sites exposed on GQDs surface. Therefore, it is impossible to completely rule out the negative effect of oxygen defects on their quantum efficiency. In the solution of high or low pH value, the free zigzag sites existing in periphery and oxygen-containing functional groups chemisorbed on basal plane would undergo deprotonation/protonation process. Therefore, the emissive state becomes inactive in PL, which explains the low pH tolerance of GQDs.<sup>16, 25</sup>

Here, AGQDs were fabricated from PAGenes by solvothermal route. According to the proposed cutting mechanism (Scheme 1), the micrometer-sized graphene sheets preferred breaking along the lines of alkylated C-C single bonds, giving rise to the ultrafine AGQDs. Unlike the periphery of GQDs, which contains free (zigzag and armchair) and functionalized edges, the edges of AGQDs were primarily terminated by alkyl groups. In addition, although the decoration of alkyl groups is reasonable, the basal plane of AGQDs process negligible oxygen defects as confirmed by XPS and FTIR analysis (Fig. 5). Therefore, the most possible origins associated with the low pH tolerance of GQDs such as the deprotonation/protonation process of free zigzag sites and oxygen-containing functional groups would basically be excluded. This may explain the greatly improved pH tolerance of AGQDs in the solution of high or low pH value. The structural characteristics of AGQDs also indicate that the origin of blue emission has no concern with oxygen-containing functional groups which commonly induced green PL in GQDs. In the basal plane of AGQDs, the functionalization of alkyl groups converted the modified carbon from  $sp^2$  hybridization to  $sp^3$ , resulting in the distortion of  $\pi$ -conjugated system. Although the mechanism details are probably more complex, we attribute the PL of AGQDs to the combination effect of intrinsic state and  $sp^3$ -defects related localized electronic states surrounding the alkylation sites. On one hand, non-radiative process was

extremely suppressed in the oxygen-defect-free AGQDs, leading to the enhanced intrinsic state emission and then higher quantum yield. On the other hand, PL emission derived from  $sp^3$  defects is generally bright, which may contribute to the efficient emission of AGQDs.<sup>48</sup> However, the individual contribution of each aspect on the PL properties of AGQDs is awaiting discovery.

To confirm the effect of oxygen-containing functional groups on the PL properties of GQDs, the synthesized AGQDs were performed oxidation using modified Hummers method.<sup>41</sup> Their optical properties were explored by means of UV-Vis absorbance, PL, and quantum yield. For the resultant oxidized AGQDs (OAGQDs), the surface oxygen-containing functional groups were clearly proved by XPS and FTIR analysis (Fig. S10a-c). The increased Raman  $I_D/I_G$  ratio from 1.1 to 1.3 provided further confirmation for the surface functionalization during oxidation (Fig. S10d). As shown in Fig. S11, OAGQDs dispersed in water process similar excitation-dependent PL behavior as that of AGQDs, while the PL peak under optimal excitation shifts from 440 nm to 445 nm. Since the resultant OAGQDs process similar size distribution as that of AGQDs (Fig. S12), the red-shift of PL wavelength can be explained by the extra contribution of oxygen-containing functional groups in OAGQDs. However, the significant decreasing in quantum yield from 65% to 8.6% is completely unexpected (Table S1).

Due to the upconversion PL properties, GQDs are promising candidates for the design of photocatalyst to harness the visible spectrum of sunlight.<sup>19</sup> We fabricated AGQDs and P25 composites by simply mixing them together in aqueous solution, followed by heating treatment at 150 °C for 6 h. The distinct color change from pure white to light yellow implies the adsorption of AGQDs on the surface of  $TiO_2$  nanoparticles. Fig. 6 shows the SEM image of the as-prepared AGQDs-P25 nanocomposites and the EDS element mapping data of C, O, and Ti elements, indicating that the element of C, O, and Ti were uniformly distributed in AGQDs-P25 nanocomposites. The XRD patterns of pure P25, AGQDs and the as-prepared AGQDs-P25 nanocomposites are shown in Fig. 7a. The observation of broad (002) diffraction peak

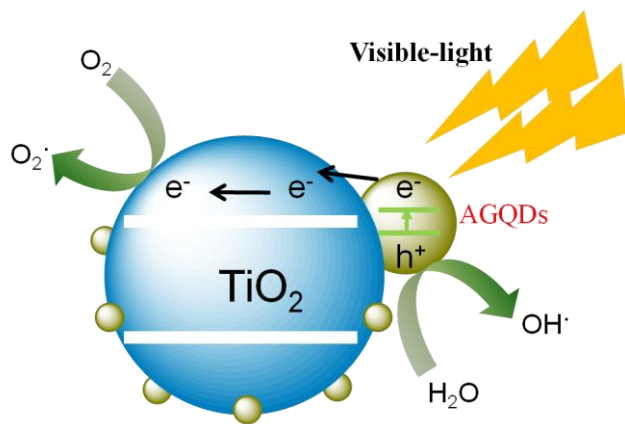


**Fig. 8** The proposed photocatalytic mechanism of AGQDs-TiO<sub>2</sub> nanocomposites under visible light irradiation.

associated with AGQDs in AGQDs-P25 nanocomposites further confirms the incorporation of AGQDs into P25.<sup>16</sup> The UV-Visible diffuse reflectance spectrum of pure P25 (Fig. 7b) shows strong UV absorption ascribed to the electron excitation from the TiO<sub>2</sub> valence band (VB) to the conduction band (CB). Upon combination with AGQDs, the spectrum shows a notable enhancement in light absorption from UV to visible and near IR, particularly in the region of 400-700 nm.

The photocatalytic activity of AGQDs-P25 was evaluated by the degradation of Rhodamine B under visible light (> 420 nm) irradiation. Fig. 7c plots the Rhodamine B concentration versus irradiation time for different catalysts. It can be seen that the photodegradation efficiency of AGQDs-P25 nanocomposites within 90 min is up to 93%, whereas the efficiency of pure P25 and AGQDs is only 25% and 11%, respectively. The pseudo-first-order reaction constant for the degradation of Rhodamine B on AGQDs-P25 is 0.0289 min<sup>-1</sup>, which is 5.9 and 22 times higher than that of pure P25 (0.0049 min<sup>-1</sup>) and AGQDs (0.0013 min<sup>-1</sup>), respectively. These results indicate that pure P25 and AGQDs have very limited photocatalytic activity under visible light. The excellent photocatalytic activity of AGQDs-P25 composites should be attributed to the interaction between AGQDs and TiO<sub>2</sub>.

Lee *et al.* showed that the visible-light-responding photocatalytic activities of GQDs/TiO<sub>2</sub> composites were attributed to the upconversion emission of GQDs.<sup>19</sup> Under visible light irradiation, the upconversion PL emission of GQDs excited TiO<sub>2</sub> to form electron/hole (e<sup>-</sup>/h<sup>+</sup>) pairs. However, this is not the case for the present AGQDs-P25 photocatalysts. As shown in Fig. 2d, the upconversion emission wavelengths of AGQDs excited by long-wavelength light are larger than 420 nm. Therefore, the upconversion emission of AGQDs is inefficient to excite the photocatalysis of TiO<sub>2</sub>. AGQDs probably play a role of photosensitizer in the degradation of Rhodamine B. As shown in Fig. 8, we expect that AGQDs absorb the visible light and the electrons are excited to the excited state, resulting in the formation of electron/hole (e<sup>-</sup>/h<sup>+</sup>) pairs. Since the AGQDs are firmly attached on the surface of TiO<sub>2</sub>, the photogenerated electrons efficiently transfer to the TiO<sub>2</sub> nanocrystals. As an n-type semiconductor, P25 TiO<sub>2</sub> tends to accept the photogenerated electrons and subsequently convert into other reactive oxidative species. The highly active holes left on the surface of AGQDs further oxidize water to produce OH· radicals, which would

eventually decompose the dye molecule (Rhodamine B) in water into CO<sub>2</sub> and H<sub>2</sub>O.

## Conclusions

In summary, AGQDs were fabricated from PAGenes by solvothermal route. The synthesized AGQDs exhibit excellent dispersibility in water and common organic solvents without further surface modification. In addition, the AGQDs process pH-independent and ultra-bright PL with quantum yield up to 65%. Structural and chemical composition characterization including XPS, FTIR, and Raman indicates that the AGQDs are nearly oxygen-defect-free, decorated with alkyl groups on edges and basal plane, which may contribute to their pH-independent and ultra-bright PL behaviors. The excellent photocatalytic performance of AGQDs-P25 nanocomposites indicates that these AGQDs could improve the use of visible light for environmental therapy.

## Acknowledgements

This work was supported by the National Key Basic Research Program of China (2013CB933901), the National Natural Science Foundation of China (No. 21171140, 21021061, 21031004, U1205111), the Natural Science Foundation of Fujian Province of China (No. 2013J01056), and the Fundamental Research Funds for the Central Universities.

## Notes and references

1. A. K. Geim and K. S. Novoselov, *Nat. Mater.*, 2007, **6**, 183-191.
2. T. Gokus, R. R. Nair, A. Bonetti, M. Bohmler, A. Lombardo, K. S. Novoselov, A. K. Geim, A. C. Ferrari and A. Hartschuh, *ACS Nano*, 2009, **3**, 3963-3968.
3. G. Eda, Y.-Y. Lin, C. Mattevi, H. Yamaguchi, H.-A. Chen, I. S. Chen, C.-W. Chen and M. Chhowalla, *Adv. Mater.*, 2010, **22**, 505-509.
4. K. P. Loh, Q. Bao, G. Eda and M. Chhowalla, *Nat. Chem.*, 2010, **2**, 1015-1024.
5. L. A. Ponomarenko, F. Schedin, M. I. Katsnelson, R. Yang, E. W. Hill, K. S. Novoselov and A. K. Geim, *Science*, 2008, **320**, 356-358.
6. C. O. Girit, J. C. Meyer, R. Erni, M. D. Rossell, C. Kisielowski, L. Yang, C.-H. Park, M. F. Crommie, M. L. Cohen, S. G. Louie and A. Zettl, *Science*, 2009, **323**, 1705-1708.
7. K. A. Ritter and J. W. Lyding, *Nat. Mater.*, 2009, **8**, 235-242.
8. J. Shen, Y. Zhu, X. Yang and C. Li, *Chem. Commun.*, 2012, **48**, 3686-3699.
9. Z. Zhang, J. Zhang, N. Chen and L. Qu, *Energy Environ. Sci.*, 2012, **5**, 8869-8890.
10. L. Li, G. Wu, G. Yang, J. Peng, J. Zhao and J.-J. Zhu, *Nanoscale*, 2013, **5**, 4015-4039.
11. Y. Li, Y. Hu, Y. Zhao, G. Shi, L. Deng, Y. Hou and L. Qu, *Adv. Mater.*, 2011, **23**, 776-780.
12. X. Yan, X. Cui, B. Li and L.-s. Li, *Nano Lett.*, 2010, **10**, 1869-1873.
13. V. Gupta, N. Chaudhary, R. Srivastava, G. D. Sharma, R. Bhardwaj and S. Chand, *J. Am. Chem. Soc.*, 2011, **133**, 9960-9963.
14. X. Sun, Z. Liu, K. Welscher, J. T. Robinson, A. Goodwin, S. Zaric and H. Dai, *Nano Res.*, 2008, **1**, 203-212.

15. S. Zhu, J. Zhang, C. Qiao, S. Tang, Y. Li, W. Yuan, B. Li, L. Tian, F. Liu, R. Hu, H. Gao, H. Wei, H. Zhang, H. Sun and B. Yang, *Chem. Commun.*, 2011, **47**, 6858-6860.
16. J. Peng, W. Gao, B. K. Gupta, Z. Liu, R. Romero-Aburto, L. Ge, L. Song, L. B. Alemany, X. Zhan, G. Gao, S. A. Vithayathil, B. A. Kaiparettu, A. A. Marti, T. Hayashi, J.-J. Zhu and P. M. Ajayan, *Nano Lett.*, 2012, **12**, 844-849.
17. D. Wang, L. Wang, X. Dong, Z. Shi and J. Jin, *Carbon*, 2012, **50**, 2147-2154.
18. L. Fan, Y. Hu, X. Wang, L. Zhang, F. Li, D. Han, Z. Li, Q. Zhang, Z. Wang and L. Niu, *Talanta*, 2012, **101**, 192-197.
19. S. Zhuo, M. Shao and S.-T. Lee, *ACS Nano*, 2012, **6**, 1059-1064.
20. D. Pan, C. Xi, Z. Li, L. Wang, Z. Chen, B. Lu and M. Wu, *J. Mater. Chem. A*, 2013, **1**, 3551-3555.
21. X. Feng, W. Pisula and K. Muellen, *Pure Appl. Chem.*, 2009, **81**, 2203-2224.
22. X. Yan, X. Cui and L.-s. Li, *J. Am. Chem. Soc.*, 2010, **132**, 5944-5945.
23. J. Wu, Z. Tomovic, V. Enkelmann and K. Muellen, *J. Org. Chem.*, 2004, **69**, 5179-5186.
24. J. Lu, P. S. E. Yeo, C. K. Gan, P. Wu and K. P. Loh, *Nat. Nanotechnol.*, 2011, **6**, 247-252.
25. D. Pan, J. Zhang, Z. Li and M. Wu, *Adv. Mater.*, 2010, **22**, 734-738.
26. D. Pan, L. Guo, J. Zhang, C. Xi, Q. Xue, H. Huang, J. Li, Z. Zhang, W. Yu, Z. Chen, Z. Li and M. Wu, *J. Mater. Chem.*, 2012, **22**, 3314-3318.
27. S. Zhu, J. Zhang, X. Liu, B. Li, X. Wang, S. Tang, Q. Meng, Y. Li, C. Shi, R. Hu and B. Yang, *RSC Adv.*, 2012, **2**, 2717-2720.
28. J.-H. Shen, Y.-H. Zhu, C. Chen, X.-L. Yang and C.-Z. Li, *Chem. Commun.*, 2011, **47**, 2580-2582.
29. J. Shen, Y. Zhu, X. Yang, J. Zong, J. Zhang and C. Li, *New J. Chem.*, 2012, **36**, 97-101.
30. H. Tetsuka, R. Asahi, A. Nagoya, K. Okamoto, I. Tajima, R. Ohta and A. Okamoto, *Adv. Mater.*, 2012, **24**, 5333-5338.
31. C. Y. Kang, L. L. Fan, S. Chen, Z. L. Liu, P. S. Xu and C. W. Zou, *Appl. Phys. Lett.*, 2012, **100**, 251604/251601-251604/251605.
32. X. Zhou, Y. Zhang, C. Wang, X. Wu, Y. Yang, B. Zheng, H. Wu, S. Guo and J. Zhang, *ACS Nano*, 2012, **6**, 6592-6599.
33. D. B. Shinde and V. K. Pillai, *Chem. - Eur. J.*, 2012, **18**, 12522-12528, S12522/12521-S12522/12529.
34. L. Lin and S. Zhang, *Chem. Commun.*, 2012, **48**, 10177-10179.
35. Y. Dong, C. Chen, X. Zheng, L. Gao, Z. Cui, H. Yang, C. Guo, Y. Chi and C. M. Li, *J. Mater. Chem.*, 2012, **22**, 8764-8766.
36. R. Ye, C. Xiang, J. Lin, Z. Peng, K. Huang, Z. Yan, N. P. Cook, E. L. G. Samuel, C.-C. Hwang, G. Ruan, G. Ceriotti, A.-R. O. Raji, A. A. Marti and J. M. Tour, *Nat. Commun.*, 2013, **4**, 3943/3941-3943/3946.
37. F. Liu, M.-H. Jang, H. D. Ha, J.-H. Kim, Y.-H. Cho and T. S. Seo, *Adv. Mater.*, 2013, **25**, 3657-3662.
38. S. L. Deng, Y. Zhang, A. H. Brozen, P. Banerjee, M. L. Mayes, W.-A. Chiou, R. G. W., G. C. Schatz and Y. H. Wang, *Nat. Commun.*, 2011, **2**, 10.1038/ncomms1384
39. L. Feng, Y.-W. Liu, X.-Y. Tang, Y. Piao, S.-F. Chen, S.-L. Deng, S.-Y. Xie, Y. Wang and L.-S. Zheng, *Chem. Mater.*, 2013, **25**, 4487-4496.
40. S. L. Deng, A. H. Brozen, Y. Zhang, Y. M. Piao and Y. H. Wang, *Chem. Commun.*, 2011, **47**, 758-760.
41. W. S. Hummers, Jr. and R. E. Offeman, *J. Am. Chem. Soc.*, 1958, **80**, 1339.
42. A. C. Ferrari, J. C. Meyer, V. Scardaci, C. Casiraghi, M. Lazzeri, F. Mauri, S. Piscanec, D. Jiang, K. S. Novoselov, S. Roth and A. K. Geim, *Phys. Rev. Lett.*, 2006, **97**, 187401/187401-187401/187404.
43. Y.-W. Liu, M.-X. Guan, L. Feng, S.-L. Deng, J.-F. Bao, S.-Y. Xie, Z. Chen, R.-B. Huang and L.-S. Zheng, *Nanotechnology*, 2013, **24**, 025604/025601-025604/025610.
44. Z. Li, W. Zhang, Y. Luo, J. Yang and J. G. Hou, *J Am Chem Soc*, 2009, **131**, 6320-6321.
45. F. Liang, L. B. Alemany, J. M. Beach and W. E. Billups, *J. Am. Chem. Soc.*, 2005, **127**, 13941-13948.
46. F. Liang, A. K. Sadana, A. Peera, J. Chattopadhyay, Z. Gu, R. H. Hauge and W. E. Billups, *Nano Lett.*, 2004, **4**, 1257-1260.
47. J. Berashevich and T. Chakraborty, *Phys. Rev. B: Condens. Matter Mater. Phys.*, 2011, **83**, 195442/195441-195442/195446.
48. L. Cao, M. J. Mezziani, S. Sahu and Y.-P. Sun, *Acc. Chem. Res.*, 2013, **46**, 171-180.
49. S. Zhu, J. Zhang, S. Tang, C. Qiao, L. Wang, H. Wang, X. Liu, B. Li, Y. Li, W. Yu, X. Wang, H. Sun and B. Yang, *Adv. Funct. Mater.*, 2012, **22**, 4732-4740.
50. L. Wang, S.-J. Zhu, H.-Y. Wang, S.-N. Qu, Y.-L. Zhang, J.-H. Zhang, Q.-D. Chen, H.-L. Xu, W. Han, B. Yang and H.-B. Sun, *ACS Nano*, 2014, **8**, 2541-2547.
51. D. Qu, M. Zheng, P. Du, Y. Zhou, L. Zhang, D. Li, H. Tan, Z. Zhao, Z. Xie and Z. Sun, *Nanoscale*, 2013, **5**, 12272-12277.
52. Z. L. Wu, M. X. Gao, T. T. Wang, X. Y. Wan, L. L. Zheng and C. Z. Huang, *Nanoscale*, 2014, **6**, 3868-3874.
53. Y. Dong, H. Pang, H. B. Yang, C. Guo, J. Shao, Y. Chi, C. M. Li and T. Yu, *Angew. Chem., Int. Ed.*, 2013, **52**, 7800-7804.
54. Y.-P. Sun, B. Zhou, Y. Lin, W. Wang, K. A. S. Fernando, P. Pathak, M. J. Mezziani, B. A. Harruff, X. Wang, H. Wang, P. G. Luo, H. Yang, M. E. Kose, B. Chen, L. M. Veca and S.-Y. Xie, *J. Am. Chem. Soc.*, 2006, **128**, 7756-7757.
55. P. Luo, Z. Ji, C. Li and G. Shi, *Nanoscale*, 2013, **5**, 7361-7367.
56. Z.-b. Qu, X. Zhou, L. Gu, R. Lan, D. Sun, D. Yu and G. Shi, *Chem. Commun.*, 2013, **49**, 9830-9832.
57. L.-L. Li, J. Ji, R. Fei, C.-Z. Wang, Q. Lu, J.-R. Zhang, L.-P. Jiang and J.-J. Zhu, *Adv. Funct. Mater.*, 2012, **22**, 2971-2979, S2971/2971-S2971/2975.
58. X. Wu, F. Tian, W. Wang, J. Chen, M. Wu and J. X. Zhao, *J. Mater. Chem. C*, 2013, **1**, 4676-4684.